(2)

AD-A210 846

DOCUMENTATION PAGE

Form Approved
OMB No. 0704-0188

THE FILE COPY

ELECTE
MAR 2 3 1989
S D

Unclassified	1b. RESTRICTIVE MARKINGS: None
2a. SECURITY CLASSIFICATION AUTHORITY	3. DISTRIBUTION/AVAILABILITY OF REPORT: Approved for public release; distribution is unlimited.
2b. DECLASSIFICATION/DOWNGRADING SCHEDULE	
4. PERFORMING ORGANIZATION REPORT NUMBER: JA 243:043:88	5. MONITORING ORGANIZATION REPORT NUMBER(S): JA 243:043:88
6a. NAME OF PERFORMING ORGANIZATION: NORDA; 6b. OFFICE SYMBOL (If applicable): 243	7a. NAME OF MONITORING ORGANIZATION: Ocean Science Directorate
6c. ADDRESS (City, State, and ZIP Code): Stennis Space Center, MS 39529-5004	7b. ADDRESS (City, State, and ZIP Code): Stennis Space Center, MS 39529-5004
8a. NAME OF FUNDING/SPONSORING ORGANIZATION: NORDA/ONT; 8b. OFFICE SYMBOL (If applicable): 243	9. PROCUREMENT INSTRUMENT IDENTIFICATION NUMBER
8c. ADDRESS (City, State, and ZIP Code): Stennis Space Center, MS 39529-5004	10. SOURCE OF FUNDING NUMBERS

PROGRAM ELEMENT NO.	PROJECT NO.	TASK NO.	WORK UNIT ACCESSION NO.
602435N	3511	JOY	DN259005
601153N	3207	330	DN294409

11. TITLE (Include Security Classification)
High-frequency acoustic backscattering from a coarse shell ocean bottom

12. PERSONAL AUTHOR(S)
S. Stanic, K.B. Briggs, P. Fleicsher, W.B. Sawyer, and R.I. Ray

13a. TYPE OF REPORT	13b. TIME COVERED	14. DATE OF REPORT (Year, Month, Day)	15. PAGE COUNT
Journal Article	FROM _____ TO _____	1989, January	12

16. SUPPLEMENTARY NOTATION

17. COSATI CODES			18. SUBJECT TERMS (Continue on reverse if necessary and identify by block number)
FIELD	GROUP	SUB-GROUP	High-Frequency Acoustics Ocean Bottom Scattering Sea Floor Roughness

19. ABSTRACT (Continue on reverse if necessary and identify by block number)

Acoustic bottom backscattering measurements were taken in a coarse shelly area 27 miles east of Jacksonville, Florida. Data from sidescan sonar, underwater television, stero photography, high-resolution bathymetry, and sediment core analysis were used t locate and classify the experimental area. Bottom backscattering measurements were made as a function of frequency (20-180kHz), grazing angle (5°-30°), and azimuthal angle. Backscattering strengths were found to follow Lambert's law, had a slight negative frequency dependence, and were consistent with measurements taken in other shelly areas. There was no azimuthal dependence of the scattered signals over the range of grazing angles and frequencies used. Bottom roughness has a Gaussian distribution and the ping-to-ping scattering signal envelope distributions were non-Rayleigh. Comparison of scattering strenths from several shelly areas showed little correlation with measured rms roughness. Scattering strength predictions made using a composite foughness model developed by Jackson et al. [J. Society Am. 79, 1410-1422 (1986)] were compared to scattering strength measurements taken at 20,40, and 60 kHz.

20. DISTRIBUTION/AVAILABILITY OF ABSTRACT	21. ABSTRACT SECURITY CLASSIFICATION
☐ UNCLASSIFIED/UNLIMITED ☒ SAME AS RPT. ☐ DTIC USERS	Unclassified

22a. NAME OF RESPONSIBLE INDIVIDUAL	22b. TELEPHONE (Include Area Code)	22c. OFFICE SYMBOL
Steve Stanic	601 688-5235	243

DD Form 1473, JUN 86 — Previous editions are obsolete. — SECURITY CLASSIFICATION OF THIS PAGE: Unclassified

High-frequency acoustic backscattering from a coarse shell ocean bottom

S. Stanic, K. B. Briggs, P. Fleischer, W. B. Sawyer, and R. I. Ray
Naval Ocean Research and Development Activity, Stennis Space Center, Mississippi 39529-5004

(Received 1 April 1988; accepted for publication 9 August 1988)

Acoustic bottom backscattering measurements were taken in a coarse shelly area 27 miles east of Jacksonville, Florida. Data from sidescan sonar, underwater television, stereo photography, high-resolution bathymetry, and sediment core analysis were used to locate and classify the experimental area. Bottom backscattering measurements were made as a function of frequency (20–180 kHz), grazing angle (5°–30°), and azimuthal angle. Backscattering strengths were found to follow Lambert's law, had a slight negative frequency dependence, and were consistent with measurements taken in other shelly areas. There was no azimuthal dependence of the scattered signals over the range of grazing angles and frequencies used. Bottom roughness had a Gaussian distribution and the ping-to-ping scattered signal envelope distributions were non-Rayleigh. Comparison of scattering strengths from several shelly areas showed little correlation with measured rms roughness. Scattering strength predictions made using a composite roughness model developed by Jackson *et al.* [J. Acoust. Soc. Am. **79**, 1410–1422 (1986)] were compared to scattering strength measurements taken at 20, 40, and 60 kHz.

PACS numbers: 43.30.Gv, 43.30.Hw

INTRODUCTION

A series of high-frequency acoustic bottom backscattering measurements was conducted in 26 m of water in an area 27 miles east of Jacksonville, Florida. This area was chosen because the bottom roughness was characterized solely by a high-impedance surficial layer of coarse shell. These measurements were taken as part of the Naval Ocean Research and Development Activity's (NORDA) high-frequency acoustics program. The approach of this program is to conduct a series of environmentally supported bottom scattering measurements in areas ranging from smooth, isotropic, and homogeneous to areas that are much more complex. It will then be possible to correlate acoustic scattering strengths and signal statistics with changes in ocean bottom characteristics. The Jacksonville measurements were the second in a series made under NORDA's high-frequency program. The initial measurements were taken in a smooth, uniform area 19 miles south of Panama City, Florida.[1] The results of those measurements are serving as the basis to which the Jacksonville and all future measurements in the program will be compared.

The acoustic measurements made at Jacksonville used NORDA's acoustic instrumentation support towers.[2,3] Scattering strength measurements were made as a function of frequency (20–180 kHz), grazing angle (5°–30°), azimuthal angle, and pulse length (5–10 ms). The acoustic measurements were supported by sidescan sonar mapping, sediment core analysis, stereo photography, and underwater television. This article presents scattering strength estimates and model comparisons as a function of acoustic and environmental parameters.

A number of comprehensive studies have been published documenting scattering strength estimates versus grazing angle in the 20- to 470-kHz range.[1,4-12] Typically, bottom scattering has been correlated with four general bottom types: mud, sand, gravel, and rock. Scattering measurements within each general bottom type have shown little correlation with particle or grain size.[11] Within each general sediment-type scattering strength estimates have varied by 10–20 dB.

These studies have shown that bottom backscattering is a function of $\sin^n \theta_g$, where θ_g is the grazing angle and n is a number between 1 and 2 (Lambert's law). For sandy sediments, scattering strength increases slightly with frequency.[7,11,12] Measurements in other shallow-water areas have shown little or no frequency dependence.[6,8] Other measurements made in shallow water have shown little dependence on measured rms bottom roughness.[1]

I. ENVIRONMENTAL MEASUREMENTS

In order to locate the experimental area, a detailed environmental survey was conducted prior to the acoustic scattering measurements. On the basis of prior investigations and detailed bathymetry gathered by the National Ocean Survey, two potential candidate areas with gravel-sized sediments were selected.[13-15] The major systems used in these surveys are described in Stanic *et al.*[2] These include a 100-kHz sidescan sonar, 3.5-kHz subbottom and Elac sediment profilers, and a 208-kHz high-resolution bathymetry system. The backscattering measurements were also supported by data provided by underwater television, stereo photography, sediment core analysis, and diver observations.

Figure 1 shows the sidescan survey tracks used to locate the experimental area. These tracks were imaged at 150-m range (300-m swath) with precision Loran-C positioning

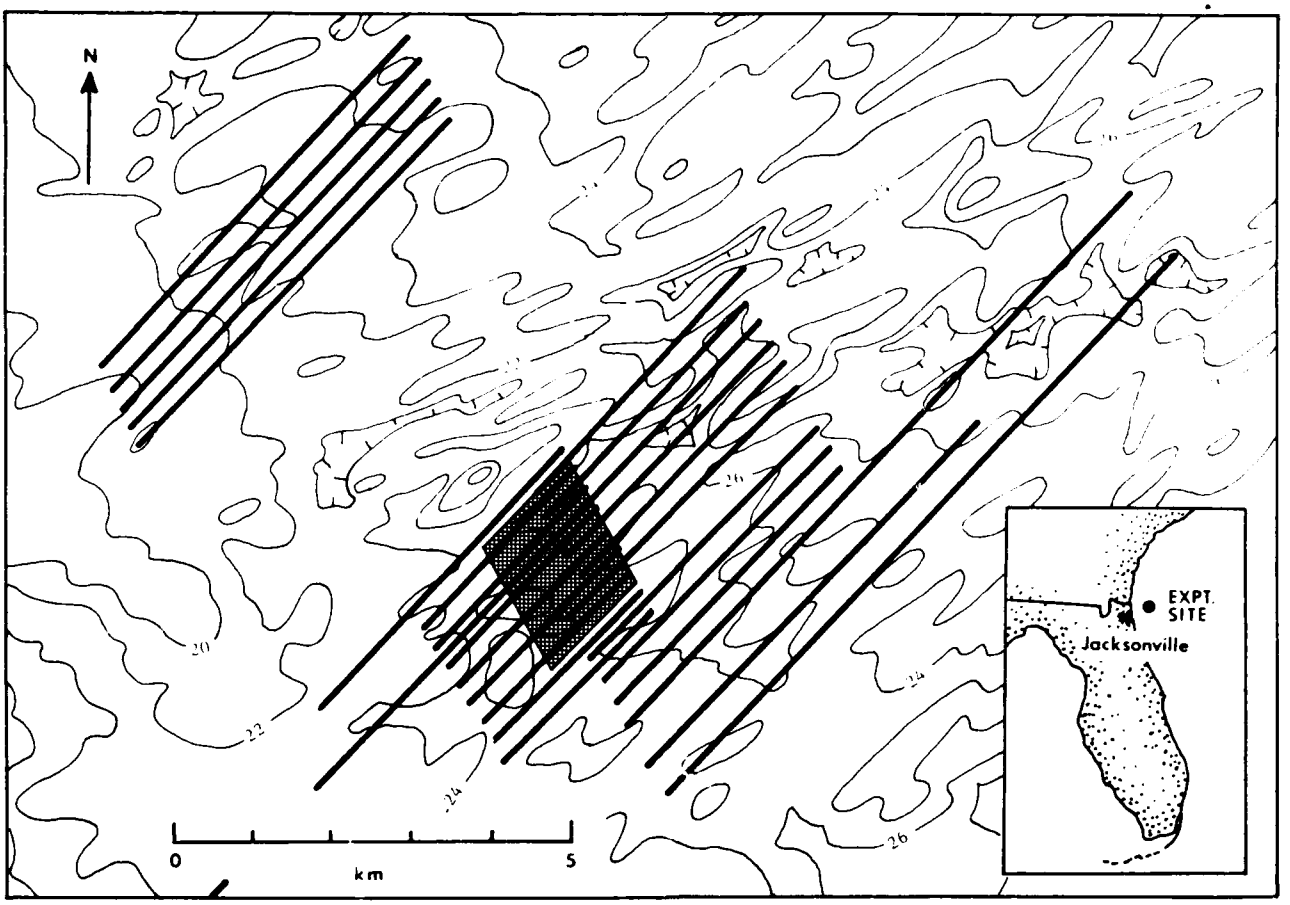

FIG. 1. Experiment site location and sidescan survey tracks. Shaded area marks location of mosaic in Fig. 2. Generalized bathymetry from National Ocean Survey (2-m isobaths).

(0.01-μs time differences). A mosaic of these swaths for the chosen experimental site and its surrounding area is shown in Fig. 2. The experiment site itself (Fig. 1) was sidescanned at 100-m range and sounded at a high line density to document small variations in bottom character and bathymetry. Figure 3 shows the computer-generated bathymetry and a three-dimensional display of the bottom morphology at the experimental site. These experimental site surveys provided data on bottom slope and large-scale roughness. These surveys were also used to extrapolate the detailed, but localized, photogrammetric and sediment property measurements over the entire area of the acoustic experiment.

The experimental site is located within the linear sand ridge morphology that typifies the inner- and midshelf seafloor of the Atlantic continental shelf from Long Island to Florida.[16] In the vicinity of the experimental site, the axial trend of the somewhat discontinuous linear sand ridges is NE/SW; amplitudes are 2–4 m, and crest-to-crest spacing is 1–2 km. This relief is superimposed on a set of broad NW/SE-trending swells that are prominent to the west and north of the site. Their relief is 6–10 m, with a 4- to 5-km spacing. The swells are a local, inherited morphology, an expression of buried and possibly eroded strata of coastal or near-shore sediments. The linear ridges are a dynamic morphology created as a seabed response to the long-term tidal and current transport over the shelf.

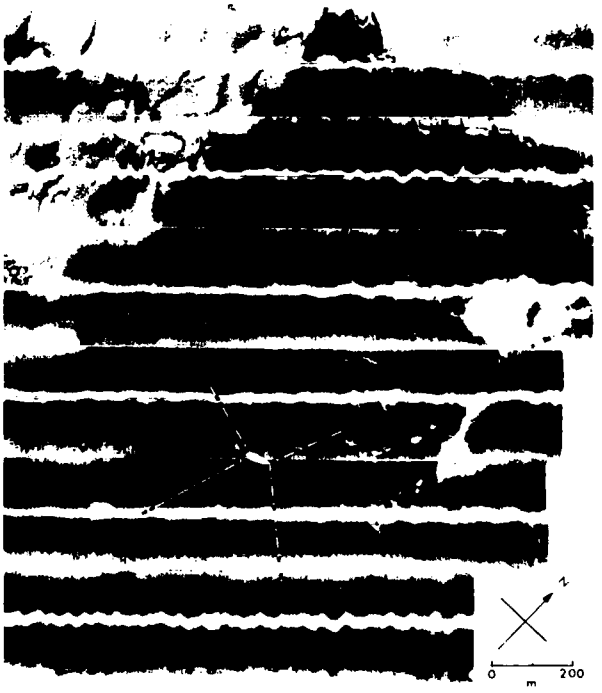

FIG. 2. Sidescan sonar mosaic of experiment site and vicinity. Ship and anchor line locations are shown. Compare with Fig. 5.

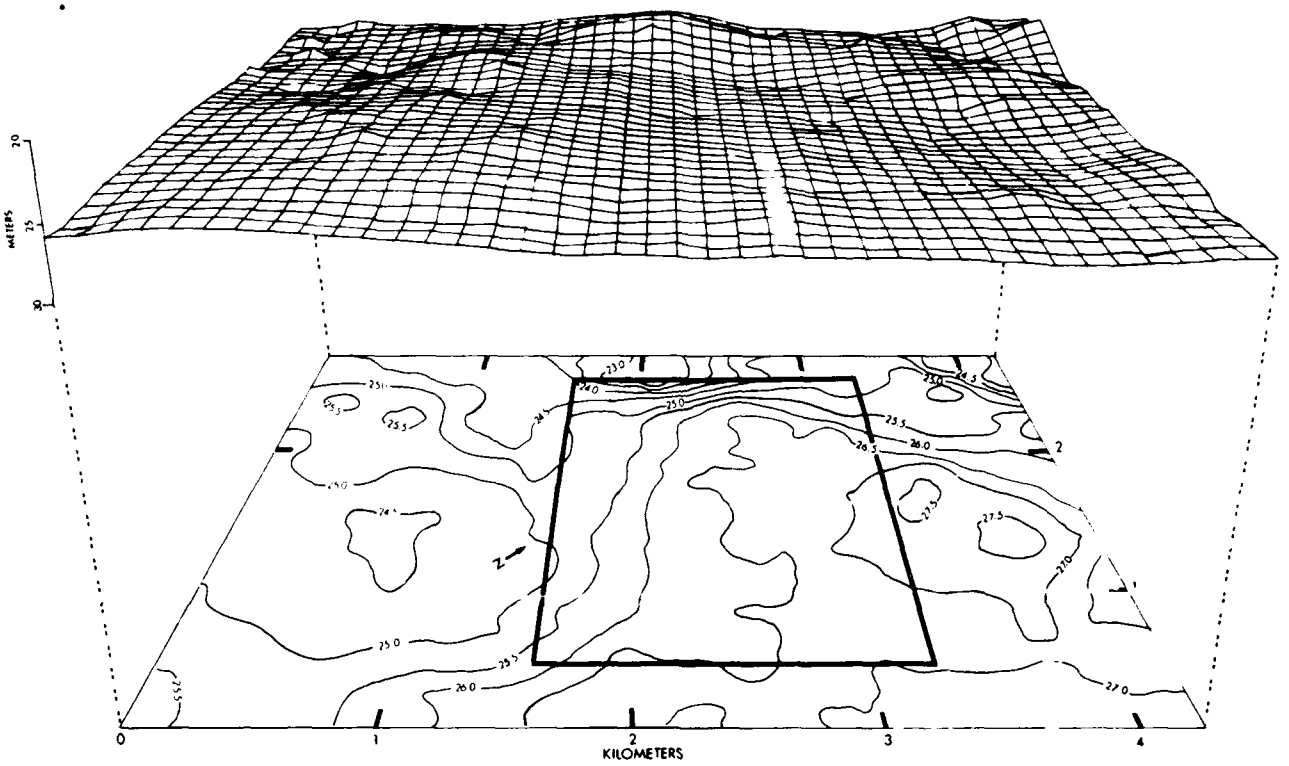

FIG. 3. High-resolution contour map (0.5-m isobaths) and relief projection of experiment site and vicinity. Relief is exaggerated. Box indicates approximate location of sidescan sonar mosaic of Fig. 2.

The site occupies an irregular NW/SE-trending depression that was formed by these swells and modified by the superimposed linear sand ridge morphology (Fig. 1). Within the site, however, there is essentially no large-scale relief other than a slight eastward tilt (Fig. 3). In this depression (and others in the vicinity), shells and coarse shell hash veneering the seabed in irregular patches produce the high reflectivity seen on the sidescan sonar mosaic (Fig. 2). A large-scale sonograph taken near the acoustic tower (Fig. 4) shows the typical backscatter pattern observed over the uniform, highly reflective seafloor. Faint lineations, at interval somewhat less than 1 m, are caused by alternating bands of coarse shell hash and shelly sand. This banding exhibits no relief. The region of lower reflectivity surrounding the site is composed of medium-grained sand. Variations in reflectivity (Fig. 5) are caused by the nonuniform occurrence of shell hash. The presence of the coarse shell material in the topographic lows of this dynamic environment indicates that it is a lag deposit produced when sand is removed by the winnowing action of currents.

Sediment core analysis and surface roughness measurements were used to classify the small-scale features of the experimental site. Sampling locations were chosen using the areal mosaic and the estimates of the acoustic patch size and location.

Divers collected sediment samples using 6.1- and 8.2-cm (i.d.) core tubes. An intact sediment–water interface within each core sample was maintained during collection, measurement, and handling. Sediment compressional wave velocity and attenuation measurements were made at 400 kHz after sediments had equilibrated with the ship's laboratory temperature, usually 24 h after collection. Values of these properties were determined at 1-cm intervals in 15 cores using an Underwater Systems, Inc. (model USI-103) transducer–receiver system.[2]

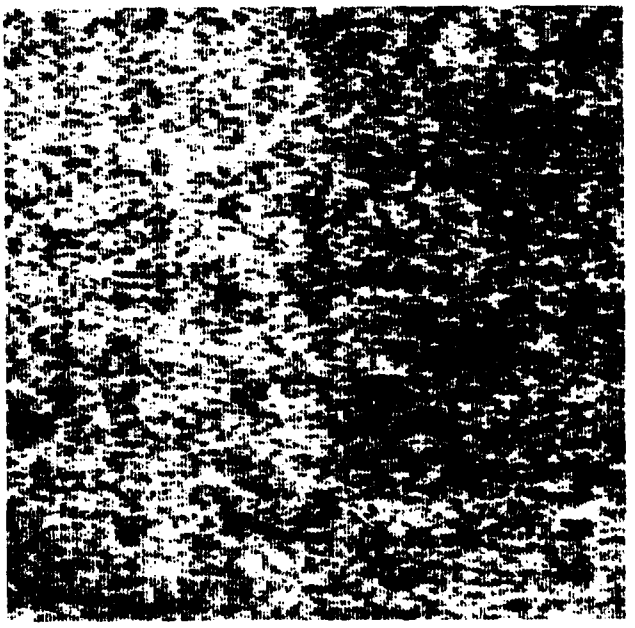

FIG. 4. Sidescan sonograph of seafloor near acoustic tower. Area is 40 × 40 m. Faint patchy lineations, 0.5–1.0 m wide (running approximately left–right on the figure), are caused by bands of coarse shell hash alternating with shelly sand. No relief is associated with the bands.

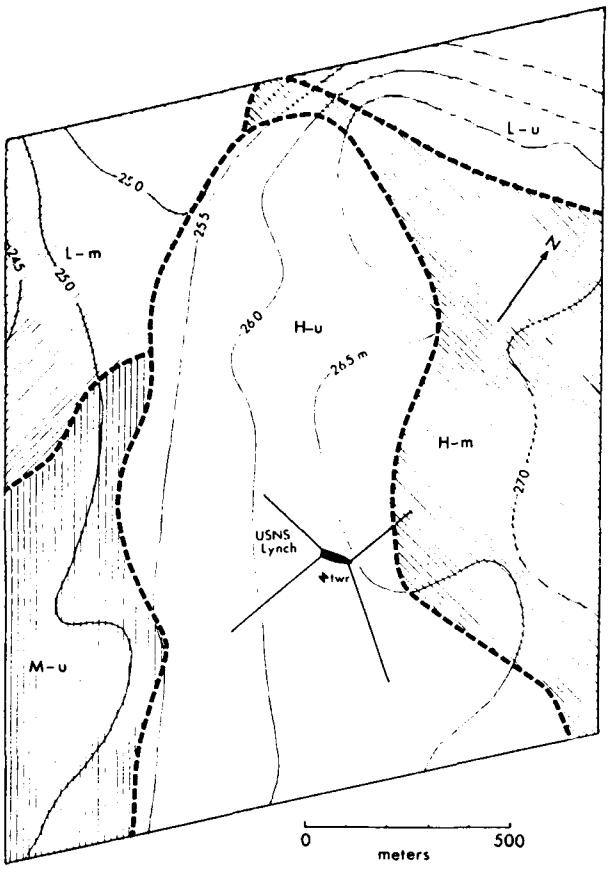

FIG. 5. Experiment setting with definition of experiment site by bathymetry and reflectivity character (H-u, high-uniform reflectivity; H-m, high mottled; M-u, medium uniform; L-u, low uniform; L-m, low mottled). Map area corresponds to sidescan mosaic of Fig. 2.

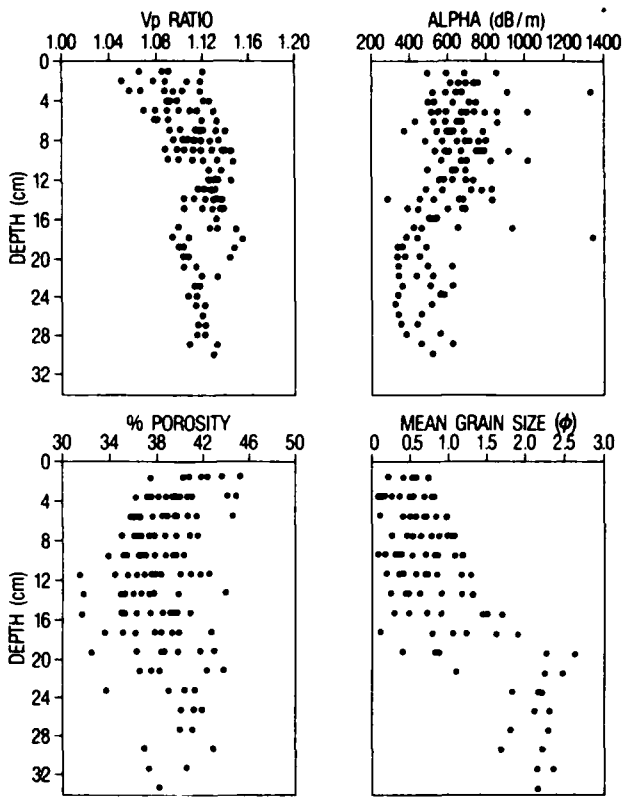

FIG. 6. Vertical distributions of sediment parameters.

Sediment compressional wave velocity at the *in situ* conditions of the experiment (27 °C, 36 ppt, 27 m) ranged from 1617–1778 m/s and averaged 1716 m/s. Compressional wave velocity ratio (measured sediment velocity divided by measured velocity for the overlying water) is independent of environmental conditions and can be used as an input for predictive acoustic scattering models.[17,27,28] A plot of compressional wave velocity ratios from 1- to 30-cm sediment depth is shown in Fig. 6. Velocity ratios averaged 1.113 with a coefficient of variation of 1.76%. A wide range of velocity ratios at the sediment surface contributed to the high variability of this parameter.

Sediment compressional wave attenuation values at 400 kHz averaged 583 dB/m and ranged from 249–1322 dB/m (coefficient of variation: 32.77%). Assuming a linear relationship between attenuation and frequency the attenuation at 20 kHz was calculated to be 29.1 dB/m. Magnitude and variability of attenuation measurements were highest in the top 18 cm of sediment (Fig. 6) and were due scattering of acoustic energy by varying amounts of mollusk shells and shell fragments.[18,19]

Measurements of sediment porosity, bulk density, average grain density, and grain-size distribution were also made. Water content was determined from the weight loss of sediment dried at 105 °C for 24 h. Sediment porosity was calculated from measurements of water content and average grain density measured on dried sediment with an air comparison pycnometer. Values of porosity were not corrected for pore-water salinity. Salt-free porosity can be obtained by multiplying the values by 1.012.

Values of sediment porosity averaged 39.0% and ranged from 32.0%–46.1% (coefficient of variation: 7.11%). The vertical distribution of porosity values decreased slightly with sediment depth (Fig. 6). Sediment density was calculated from values of porosity and average grain density and expressed as the ratio of sediment density to overlying water density. The average sediment density of 2.039 g/cm^3 yielded an average density ratio of 1.993.

Sediment grain-size distributions were measured from disaggregated samples by dry sieving for gravel- and sand-sized particles at quarter-phi intervals and by pipette for silt- and clay-sized particles. Grain-size statistics were determined from the graphic formulas of Folk and Ward.[20]

The mean grain size of sediment samples from 12 cores was 0.84 ϕ (0.557 mm), which corresponds to a coarse sand. However, detailed analysis shows the mean to be coarse skewed from medium sand by high concentrations of shell fragments, in size fractions from coarse sand (1.0 ϕ) to pebble gravel ($-4.0\,\phi$).[21] The top 18 cm of sediment is characterized by coarser material (0.61 ϕ, or 0.655 mm) and overlies a finer sediment (1.85 ϕ, or 0.277 mm) of less than 5% gravel by weight (Fig. 6). The high concentration of shells in the surficial sediment was obvious from observations and

FIG. 7. Alternating bands of coarse shell hash.

sediment surface samples taken by divers. Denser concentrations of shell hash distributed in parallel, alternating bands were oriented N/S and are evident in Fig. 7. These bands averaged 42 cm in width and had an average period of 78 cm. Despite a lack of significant elevation difference between the darker, concentrated shell bands and the lighter, sparse shell bands, differences in grain-size characteristics did exist in the top 2 cm of sediment. Gravel-size-fraction percentages of the darker bands averaged 57.5%, whereas gravel-size-fraction percentages of the lighter bands averaged only 17.8%. In addition to the larger proportion of gravel, larger fragments and a greater number of whole shells were found in the darker bands. Figure 8 shows histograms of the shell distributions in the dark and light bands.

Bottom roughness was determined from stereo photographs made with a diver-operated 35-mm stereo underwater camera (Photosea model 2000M) with a 100 W/s underwater strobe (Photosea model 1000S). Two Nikon UW-NIKKOR 28-mm lenses were separated by 61 mm, yielding a 55-×72-cm image overlap.[2]

Orientation of photographs was determined using a diver's compass and a 3-m-long tape measure. Photographic transects oriented at 150° and 240° coincided with the azimuthal directions of the acoustic source used in the experiment. Stereo photographs from two stations were analyzed. Station 103 was centered 15 m southeast of the acoustic tower and station 111 was centered 30 m southeast of the tower.

From a total of 113 bottom stereo photographic pairs, 24 representative pairs were selected for analysis. Each stereo pair was analyzed with a Seagle 90 Subsea photogrammetric stereocomparator. Calibration of the camera lenses at the focal distance used in the experiment was done by Hasselblad, the developer of the photogrammetric software. Vertical resolutions of less than 1 mm have been demonstrated in previous analyses.

Relative sediment height was determined for 128 equally spaced (0.42 cm) points along three 53.34-cm-long profiling lines in each stereo pair. In each stereo pair, the profiling lines were restricted to the central area of the image and parallel to the tape measure.

Bottom roughness was calculated as rms height (standard deviation) from the 72 sets of digitized profiling lines. The power spectral density functions were estimated for each set of 128 points using manipulations for sediment roughness data developed by D.B. Percival of the Applied Physics Laboratory, University of Washington.[22] The spectra were averaged for each photographic location (stations 103 and 111) and orientation (150° and 240°).

Although the alternating dark and light bands of shell hash created the illusion of a broadly rippled bottom (Fig. 7), stereo photographs taken at the experiment site revealed little microtopographical relief. Representative profiling lines plotting relative sediment height versus path length for the light and dark bands are shown in Fig. 9.

The rms roughness averaged 0.42 cm for all 72 profiling lines examined from the experiment site. Values of rms height for the individual digitized profiling lines ranged from 0.21–0.95 cm. Table I displays mean rms values for each location and orientation (150° and 240°). The seafloor at the experiment site was generally devoid of significant topographical features except for occasional sea urchins (*Lytechinus callipeplus*), which occur in over 5% of the photographs. Differences in mean rms height for different locations and azimuthal directions were tested by t tests of means (pooled estimate of variance). There were significant differences between the two orientations at station 111 and between stations 103 and 111 at the 150° orientation. Despite significant differences in individual groupings of data, there were no demonstrable trends in rms height for the experimental site. The absence of any obvious trends is confirmed by lack of differences in the means given in Table I.

Bottom roughness can be expressed in terms of the spatial frequency components of the relative height measure-

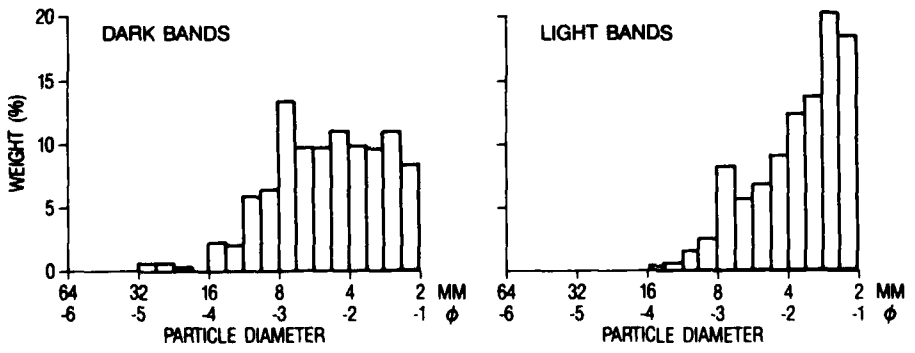

FIG. 8. Histogram distributions of surface shell size in the light and dark bands.

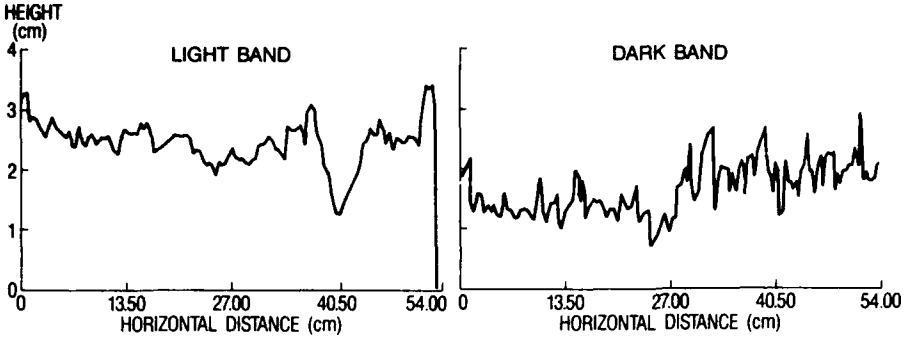

FIG. 9. Relative sediment height versus path length for the light and dark bands.

ments by estimates of the power spectral density function (wavenumber is related to spatial frequency by 2π). Periodogram estimates of power spectra for bottom roughness at the two photographic stations are presented in Fig. 10. These periodograms represent the averaging of power spectral values from 36 digitized profiling lines from each of the two azimuthal directions. Since the spectrum is two-sided, the integral of the spectrum from zero frequency to the highest (Nyquist) frequency is equal to one-half the mean-square height (roughness). The 95% confidence interval is computed from tabulated chi-square values.[23]

The slopes of the power spectra from regressions of (log) power spectrum value on (log) frequency are -1.50 and -1.44 for Fig. 10(a) and (b), respectively. Power spectra slopes at each location and at each azimuthal direction are given in Table II. An analysis of covariance for testing the equality of slopes of the power spectra reveals no significant differences between power spectra slopes for different azimuthal directions at either station. Regression slopes of 18 aggregated periodograms per block rather than ensemble-averaged periodograms were used in testing slope equality. Slope values at this site are 0.5–1.0 slope units ($\log \text{cm}^3/\log \text{cm}^{-1}$), less steep than the measured roughness power spectra in other areas.[1,18,19] Less steep power spectra slopes in this case indicate a greater proportion of power concentrated in the higher spatial frequencies.

Figure 11 shows a histogram for an average of ten roughness profiles taken at Jacksonville. A chi-square goodness-of-fit test was performed at the $\alpha = 0.05$ level of significance. The computed statistic is χ^2 and the threshold value is $\chi^2_n{:}\alpha = 0.05$. For $\chi^2 < \chi^2_n{:}\alpha = 0.05$ and $n = 44$, the roughness data passed the test, implying that the roughness is in fact Gaussian. The solid line is the Gaussian probability density function that was fitted to the data. Table III gives calculated values of the variance, skewness, and kurtosis.

In addition to measurements of the bottom parameters, temperature and sound-speed profiles were recorded every 4 h using standard CTD equipment. These data were used to generate ray plots and to determine the acoustic incident angles, insonified areas, and propagation loss values. The water column was generally isovelocity, with no large-scale temporal changes during the course of the experiment.

TABLE I. The rms roughness values (cm) for the 53.34-cm-long profiling lines obtained from stereo photographs of the seafloor at the experimental site. Values for each orientation at each station are averages of 18 profiling lines for each orientation at each station.

Photograph location	Profiling lines 150°	240°	all
103	0.450	0.394	0.423
111	0.312	0.494	0.413
Mean	0.387	0.447	0.418

II. ACOUSTIC INSTRUMENTATION

Figure 12 shows one of NORDA's acoustic instrumentation support towers. This tower is a twin-hull catamaran design with a vertical tank supporting an instrument chamber, a triaxial positioner, and a two-dimensional array mount. The array mount is a rigid tubular structure that supports the acoustic sources and hydrophones. The tower was transported to a staging area, where it was assembled and the transmitting and receiving systems installed. The USNS LYNCH was then placed in a stable four-point mooring at a position determined from the sidescan sonar mosaic.

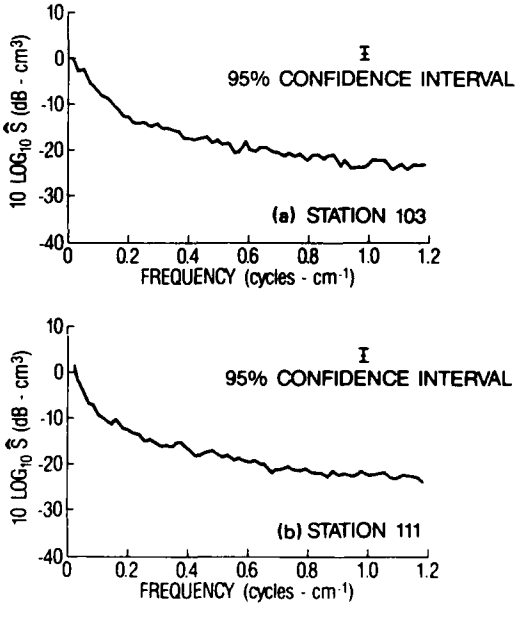

FIG. 10. Power spectra estimates for bottom roughness.

TABLE II. Slope values of regressions of (log) power spectral value on (log) frequency from sediment height data collected from stations 103 and 111 and orientations 150° and 240°.

Photograph location	Profiling lines 150°	240°	all
103	− 1.54	− 1.38	− 1.47
111	− 1.43	− 1.49	− 1.48
Mean	− 1.50	− 1.44	− 1.47

The acoustic tower was towed by a small boat to a predetermined position near the LYNCH and deployed on the ocean bottom. Divers then connected various umbilical cables between the tower and the support ship. A typical experimental configuration is shown in Fig. 13. The relationship between the moored ship, the tower, and the surrounding bottom is also detailed in Fig. 5.

The transmitting system utilized a pair of broadband parametric sources that operated from 20–180 kHz, with source levels between 187 and 214 dB *re*: 1 μPa. Beamwidths were less than 3°.

The acoustic receiving system consisted of a 16-hydrophone, two-dimensional spatial array. The hydrophones were EDO model 6660 omnidirectional elements with broadband capabilities to 250 kHz. Two elliptical filters, a buffer amplifier, and a 40-dB gain preamplifier formed an integral part of each hydrophone. The filters were needed to eliminate the high-level primary frequencies transmitted by the parametric sources.

III. ACOUSTIC DATA ANALYSIS

A single multiplexed signal containing data from 16 hydrophones and six engineering channels was recorded on a Honeywell model 101 tape recorder. Clock signals, gate pulses, transmitted waveforms, and phase-locked sampling signals were recorded on the remaining channels. During analysis, the multiplexed signal was demodulated and the narrow-band modulation outputs, centered at 5 kHz, were amplified, filtered, and converted to 12-bit A/D envelope records. For each experimental configuration, a number of sequential pings were used to form ensemble averages. A mean backscattering strength was estimated for each configuration and set of envelope data records.

TABLE III. Histogram statistics.

Variance	0.15
Skew	0.08
Kurtosis	− 0.18

The mean backscattering strength BS, in dB *re*: 1 m^2, was calculated according to the following equation:

$$BS = RL - SL + 2TL - 10 \log A,$$

where BS is the scattering strength in dB *re*: 1 m^2, RL is the received level in dB *re*: 1 μPa, SL is the source level in dB *re*: 1 μPa at 1 m along the maximum response axis, TL is the transmission loss in dB, and A is the effective insonified bottom area in m^2.

Since the beam patterns of the parametric sources were circularly symmetric, the effective insonified areas were the projection of the circular area at the 3-dB downpoints of the main beam on the bottom. This assumes that the grazing angle is constant over the instantaneous area. This is acceptable because the linear sound-speed profile did not produce any focusing or shadowing in the measurement areas. In cases where the area was pulse-length limited, the area was defined as

$$A = r\beta\,[\,(c_b\tau/2)\sec\theta_g\,],$$

where r is the horizontal range, c_b is the sound speed just above the bottom, τ is the pulse length, β is the effective beam width of the projector and receiving hydrophone in radians,[24] and θ_g is the grazing angle.

IV. BOTTOM BACKSCATTERING RESULTS

A. Grazing angle dependence

Acoustic backscattering strength measurements were made as a function of frequency, grazing angle, pulse length, and azimuthal angle. Figure 14 shows scattering strength estimates as a function of frequency (20, 40, 60, and 90 kHz) and grazing angles (5°–30°). The values for 20 kHz at this

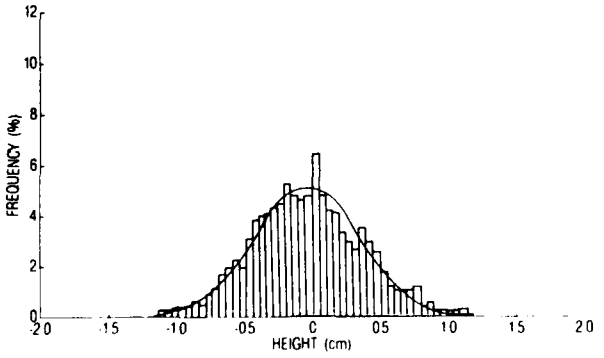

FIG. 11. Histogram of 10 averaged bottom roughness profiles.

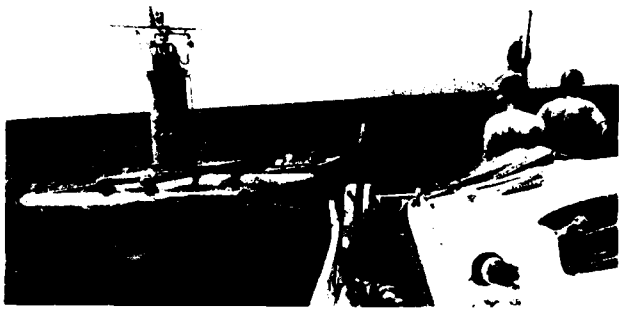

FIG. 12. Acoustic instrumentation support tower.

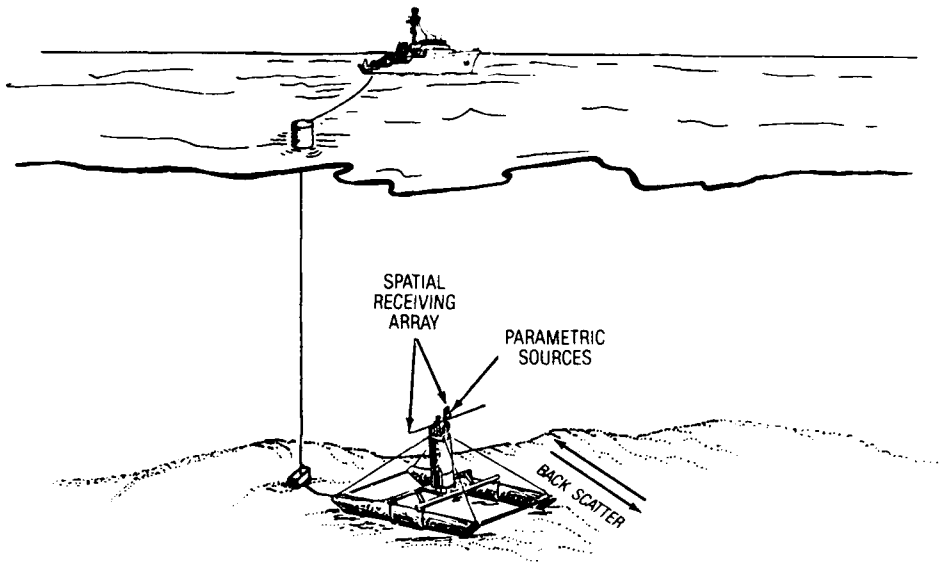

FIG. 13. Experimental configuration.

site were on average 2–3 dB lower than those reported by Roderick and Dullea[8] for an area off Long Island, which also had a shell-type bottom. Scattering strength values at 20 and 40 kHz are similar to those measured by Jackson *et al.*[10] in Puget Sound. This area was also covered with a dense layer of live shellfish. Figure 15 gives the high-frequency scattering strength estimates (110, 130, 150, and 180 kHz) as a function of grazing angle. These values have the same general functional dependence and magnitude as the low-frequency scattering strengths.

Figures 16–18 detail the scattering strength estimates as a function of azimuthal angle for different frequencies (20, 90, and 150 kHz) and grazing angles. These figures show that, even though the bottom showed bands of varying surface shell concentrations, it was not a significant factor in the azimuthal dependence of the scattering strength estimates.

Figure 19 is a comparison of the measured rms roughness versus calculated scattering strength for measurements made at Long Island,[8] Jacksonville, and Puget Sound.[10] In these areas where the bottom is covered with a dense shell layer, scattering strengths were on average 8–10 dB higher than those measured at the smooth Panama City location and showed no significant dependence on rms bottom roughness. Low grazing angle scattering strengths should be sensitive to changes in bottom roughness. However, rms roughness is a very simple description of a complex surface and provides no data on the frequency content or slopes of the roughness contours. Emphasis must be placed on describing the bottom in terms of these quantities.

Figure 20 gives representative histograms of the scattered signal envelope variations. These results are for 90 and 150 kHz and for grazing angles of 12.6° and 11.1°, respectively. A Rayleigh probability density function, calculated using the mean and variance of the scattered envelope fluctuations, is shown for comparison.[25] Table IV lists the ping-to-ping coefficient of variation for a series of 90- and 150-kHz cw pulses. These values averaged 42% and 43%, respectively. For a Rayleigh distribution this ratio is 52%.[26] Thus the data show a significant departure from a Rayleigh model. It is believed that the variances in scattering strength estimates are caused by small-scale fluctuations in the ocean's index of refraction. This departure from a Rayleigh model is consistent with narrow-beam results obtained at San Diego[9] and Charleston.[12] Knowledge of these scattering distribution

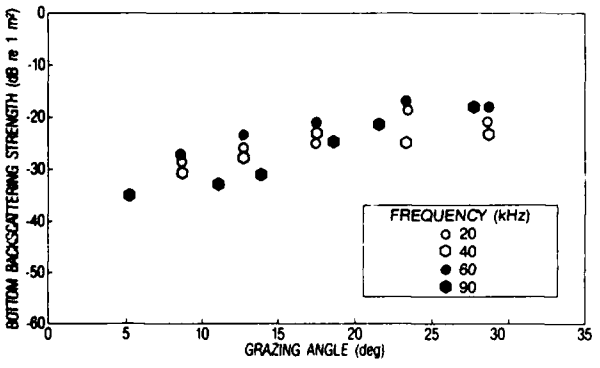

FIG. 14. Backscattering strength versus grazing angle for lower frequencies.

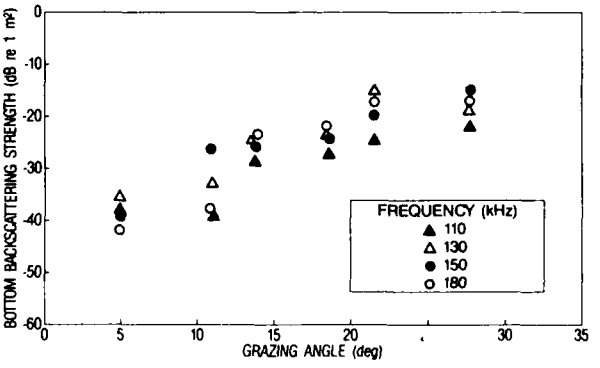

FIG. 15. Backscattering strength versus grazing angle for higher frequencies.

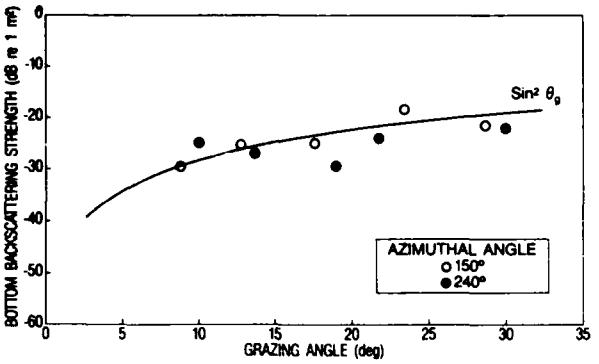

FIG. 16. Azimuthal dependence of bottom backscatter at 20 kHz.

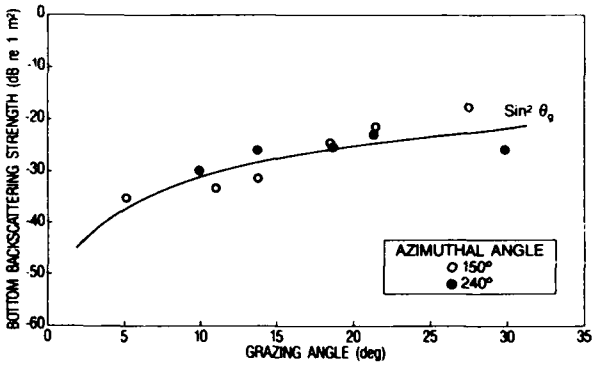

FIG. 17. Azimuthal dependence of bottom backscatter at 90 kHz.

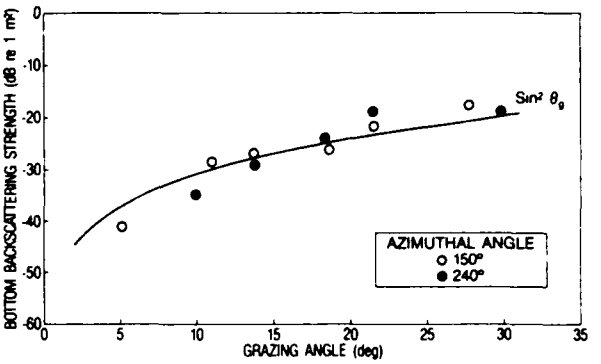

FIG. 18. Azimuthal dependence of bottom backscatter at 150 kHz.

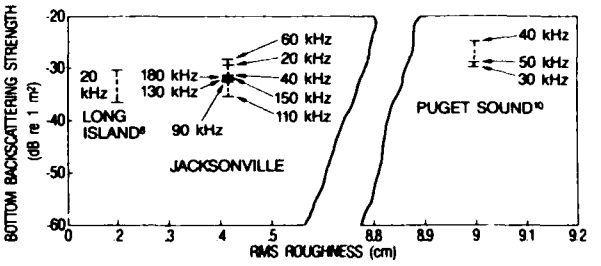

FIG. 19. Comparison of bottom backscattering strength versus rms roughness for an 8° gazing angle.

functions as a function of acoustic and environmental parameters is essential for designing optimal detection systems. A complete analysis of the statistics of the scattered signals and the bottom roughness will be presented in a future article.

Scattering strength measurements were made using 5- and 10-ms-long cw pulses. There was no apparent dependence of scattering strengths on pulse length.

B. Frequency dependence

Scattering strength can be expressed as (Lambert's law):[4]

$$\mathrm{BS} = 10\log\mu + 10\log(\sin^2\theta_g),$$

where $10\log\mu$ is the backscattering strength at normal incidence if Lambert's law is satisfied.

A $\sin^2\theta_g$ curve was fitted to each set of backscattering data. A value of $10\log\mu$, the bottom scattering characteristic, was then calculated. Typical results are shown in Figs. 16–18. Scattering strength estimates at the other frequencies also followed a $\sin^2\theta_g$ dependence. Figure 21 is a plot of the bottom scattering characteristic ($10\log\mu$), versus frequency. The error bars are the standard deviations of the measured data. The data taken at Jacksonville exhibited a weak frequency dependence of -0.75 dB/oct. Data taken by Jackson at the rough Puget Sound[10] site showed a frequency dependence of 0.8 dB/oct. The scattering strength measurements taken by Roderick and Dullea[8] showed no frequency dependence over a frequency range of 5–20 kHz. Because of

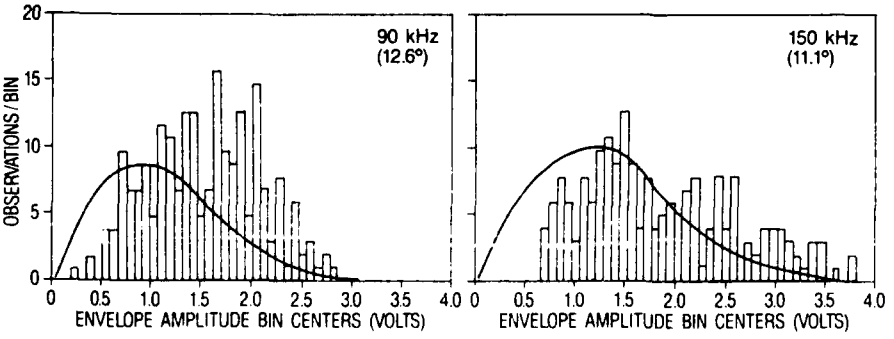

FIG. 20. Scattered signal single-ping histograms.

TABLE IV. Estimates of the envelope means, variances, and coefficient of variations.

Frequency	Envelope mean (V, η)	Variance (σ^2)	Coefficient of variation (σ/η) × 100%
kHz			
90 (12.6°)	1.88	0.46	35
	1.69	0.49	41
	1.92	0.73	45
	1.84	0.57	41
	1.86	1.04	54
	1.86	0.58	41
	1.43	0.50	49
	1.96	0.43	33
	2.03	0.63	39
	1.74	0.52	41
kHz			
150 (11.1°)	1.66	0.66	49
	1.72	0.68	48
	2.01	0.85	46
	1.91	0.50	47
	1.49	0.32	38
	1.97	0.73	43
	1.65	0.33	34
	1.42	0.47	48
	1.57	0.36	38
	1.68	0.55	44

the large roughness scales in these areas, a weak frequency dependence was expected.

A comparison of the frequency dependence at Jacksonville with those at three sandy sites is shown in Fig. 22. The sandy areas were characterized by a medium-to-fine sand with a low shell content. These curves tend to converge at frequencies between 130 and 180 kHz. This may suggest that because of sediment dynamics at the sandy areas at Panama City, San Diego, and Charleston, bottom roughness wavelengths may never be small enough to produce any frequency dependence above about 180 kHz. Very high-frequency scattering strengths taken in these areas may begin to show a frequency dependence as the acoustic wavelengths approach the actual grain sizes. However, scattering strength data above 180 kHz are needed to support this hypothesis.

V. MODEL COMPARISON

A composite roughness model developed by Jackson *et al.*[27] has been used to make high-frequency bottom backscattering strength predictions as a function of grazing angle and environmental conditions. The required environmental inputs are sediment compressional velocity ratio, sediment density ratio, sediment volume scattering parameter, one-dimensional roughness spectrum slope, and spectrum level at 1 cycle cm^{-1}. The model also calculates the range of grazing angles over which the predictions are considered valid. These are based on assumptions partitioning the roughness spectrum into its large- and small-scale parts. However, as a result of difficulty in estimating the error resulting from these assumptions, the conditions governing the boundary between large- and small-scale relief are not well defined.[27]

Predictions of bottom backscattering strength are shown in Figs. 23–25. These predictions were made for acoustic frequencies of 20, 40, and 60 kHz, a velocity ratio of 1.113, a density ratio of 1.993, a spectrum slope of -1.47, and a spectrum level of -22.25 dB cm^3. For sandy bottoms the volume scattering parameter σ_v has been estimated to be 0.002.[27,28] Figures 23–25 also compare the predicted scattering strengths with measured data. At 20 kHz, the measured data are 3–7 dB higher. If the value of σ_v is set equal to 0.01, the model predictions and measured data compare favorably above the 26° critical angle. Currently, the model does not

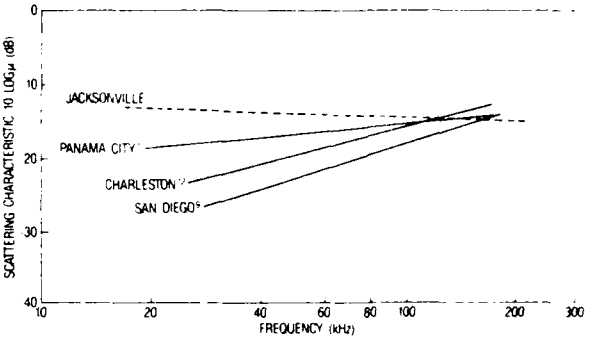

FIG. 22. Comparison of frequency dependence for Jacksonville, Panama City, Charleston, and San Diego.

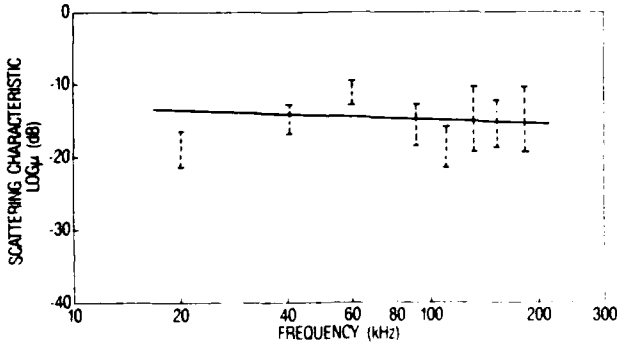

FIG. 21. Frequency dependence.

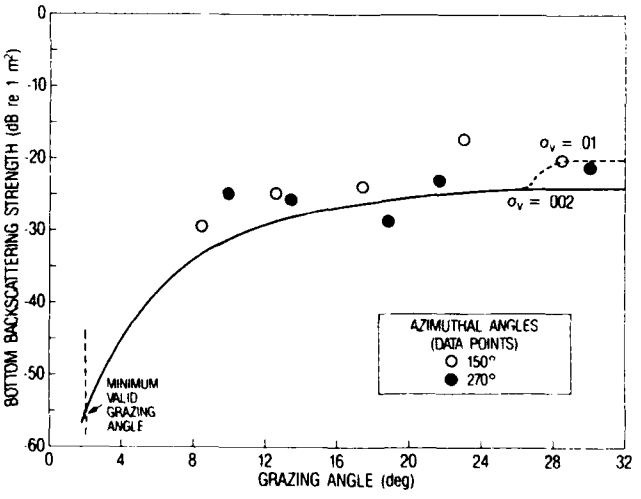

FIG. 23. Comparison of backscattering strength predictions with experimental results for 20 kHz.

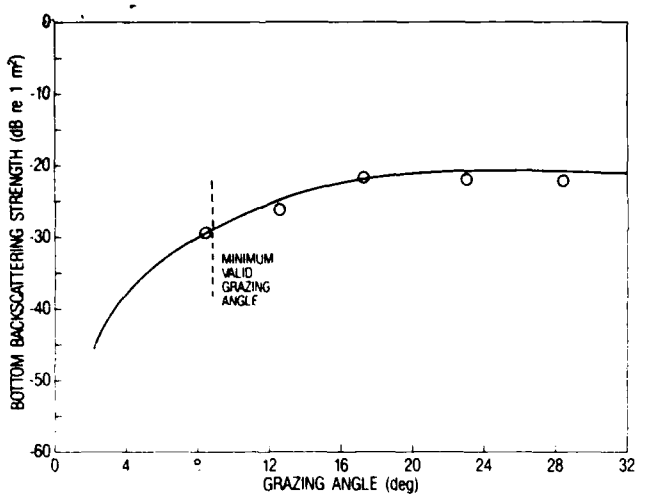

FIG. 24. Comparison of backscattering strength predictions with experimental results at 40 kHz.

allow for volume scattering below the critical angle. However, it is possible that below the critical angle there may be local penetration that could result in additional scattering from the sediment volume. This would account for the difference between the model predictions and measured data below 26°. At 40 kHz, the model predictions compare favorably with the measured data. At this frequency, the assumption of r = 0 penetration appeared to be valid. The data at 60 kHz are in good agreement with the model predictions above grazing angles of 23°, but below 23° the data are 2–6 dB lower. This may be due to difficulties in the composite roughness model at small grazing angles.

VI. SUMMARY

Geoacoustic and bottom roughness data define the significant feature of the seafloor at the Jacksonville experimental site to be coarse shell hash. Besides being a potentially strong acoustic reflector, such concentrations of shell material are responsible for considerable variation in geoacoustic measurements. Coefficients of variation for geoacoustic properties in other sandy shallow-water sites are generally lower by a factor of 2.[29]

However, most of the variation in grain-size distributions is due to vertical rather than horizontal variability. The seafloor at the experimental site is characterized by a 2-cm layer of very coarse shell hash that overlies a medium sand with significant amounts (20% by weight) of gravel-sized shell material. Sediments below 18 cm are finer, with less shell material, and do not affect backscattering at the transmitted acoustic frequencies. Variability of grain size at the sediment surface, where bands of coarser shell hash alternate with areas of sparser, less coarse shell hash, does not appear to produce any variability in the measured acoustic backscatter strengths. These shell bands were also not important enough to produce any scattering anisotropy. A comparison of scattering strengths from areas where the bottom was covered with live shellfish showed no correlation with measured rms bottom roughness.

Scattering strength estimates tended to follow Lambert's law and had a frequency dependence of -0.75 dB/oct. The measured scattering strengths at Jacksonville, Long Island,[8] and Puget Sound[10] were nearly identical even though at all sites the sediments below the coarse shell surface were different. This supports the assumption that the primary scattering mechanism, especially above 20 kHz, was the surface roughness.

Predictions using Jackson's composite roughness model did not produce a good fit to the experimental data points at 20 kHz. However, if the volume scattering parameter was increased, the model predictions and measured data did compare favorably above the critical angle. There was good agreement at 40 kHz, but the data at 60 kHz were 2–6 dB lower below a grazing angle of 23°.

During the summer of 1989, NORDA is planning a third experiment off the coast of Panama City, Florida. The surface roughness in this area will be characterized by sand waves and ripples. Additional measurements are also needed for sandy areas where there are a significant number of volume scatterers. This would allow the volume scattering parameter to be better quantified.

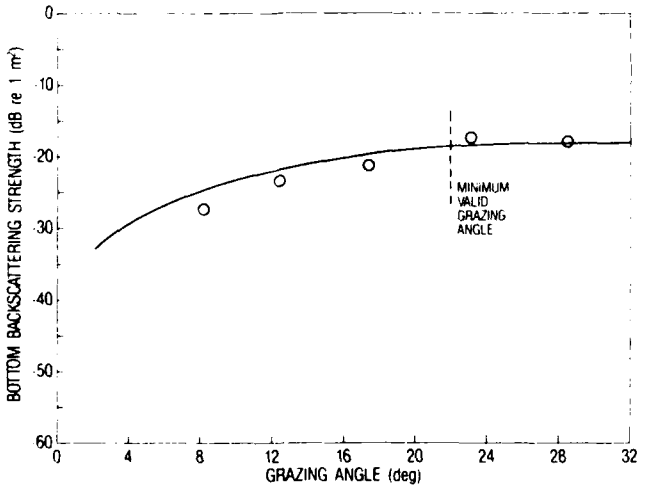

FIG. 25. Comparison of backscattering strength predictions with experimental results at 60 kHz.

ACKNOWLEDGMENTS

The authors particularly thank L. Carlton and W. Clay of the Naval Underwater Systems Center, New London, Connecticut for development of the parametric acoustic sources. We also thank R. Love and R. W. Farwell of NORDA for their helpful comments. The composite roughness model was provided by D. R. Jackson (ARL/UW). Thanks are due to the Mayport Naval Station, Mayport, Florida, for cooperation with logistics and support for staging and testing. This work was supported by the Office of Naval Research, program element 61153N, through the NORDA Defense Research Sciences Program and the Office of Naval Technology program element 62435N. NORDA contribution number 243:035:88.

[1]S. Stanic, K. B. Briggs, P. Fleischer, R. I. Ray, and W. B. Sawyer, "Shallow-water high-frequency bottom scattering off Panama City, Florida," J. Acoust. Soc. Am. **83**, 2134–2144 (1988).
[2]S. Stanic, P. Fleischer, K. B. Briggs, M. P. Richardson, and B. Eckstein, "High frequency acoustic bottom scattering experiments, part I. Instrumentation and methods," NORDA Rep. No. 178, Naval Ocean Research and Development Activity, NSTL Station, MS (January 1987).
[3]S. Stanic, B. Eckstein, B. Williams, P. Fleischer, and K. B. Briggs, "A high-frequency shallow-water acoustic measurement system," IEEE J. Ocean. Eng. **13**, 155–162 (1988).
[4]R. J. Urick, *Principles of Underwater Sound* (McGraw-Hill, New York, 1975).
[5]H.-K. Wong and W. D. Chesterman, "Bottom backscattering near grazing incidence in shallow water," J. Acoust. Soc. Am. **44**, 1713–1718 (1968).
[6]A.V. Bunchuk and Yu. Yu. Zhitkovskii, "Sound scattering by the ocean bottom in shallow-water regions (review)," Sov. Phys. Acoust. **26**, 363–370 (1980).
[7]C. M. McKinney and C. D. Anderson, "Measurements of backscattering of sound from the ocean bottom," J. Acoust. Soc. Am. **36**, 158–163 (1964).
[8]W. I. Roderick and R. K. Dullea, "High resolution bottom backscattering measurements," NUSC tech. doc. 7181, Naval Underwater Systems Center, New London, CT (June 1984).
[9]H. Boehme, N. P. Chotiros, L. D. Rolleigh, S. P. Pitt, A. L. Garcia, T. G. Goldsberry, and R. A. Lamb, "Acoustic backscattering at low grazing angles from the ocean bottom. Part I. Bottom backscattering strength," J. Acoust. Soc. Am. **77**, 962–979 (1985).
[10]D. J. Jackson, A. M. Baird, J. J. Crisp, and P. A. G. Thomson, "High-frequency bottom backscatter measurements in shallow water," J. Acoust. Soc. Am. **80**, 1188–1199 (1986).
[11]N. P. Chotiros and H. Boehme, "High frequency environmental acoustics bottom backscattering analysis," ARL-TR-86-27, Applied Research Laboratories, University of Texas at Austin (October 1986).
[12]H. Boehme, N. P. Chotiros, and D. J. Churay, "High frequency environmental acoustics bottom backscattering results," ARL-TR-85-30, Applied Research Laboratories, University of Texas at Austin (October 1985).
[13]W. P. Dillon, "Geology report for proposed Oil and Gas Lease Sale 90, continental margin off the southeastern United States," Rep. No. 83-186, U.S. Geol. Surv. Open file (1983).
[14]P. Popenoe, B. Butman, C. K. Paull, M. M. Ball, and S. L. Pfirman, "Southeastern U. S. Atlantic shelf potential geologic hazards," Map MF-1276, U.S. Geol. Surv. (1981).
[15]V. J. Henry, "Ocean bottom survey of the U.S. South Atlantic OCS Region, Marine Geology Program," Final Rep., University of Georgia (1983).
[16]D. B. Duane, M. E. Field, E. P. Meisburger, D. J. P. Swift, and S. J. Williams, "Linear shoals on the Atlantic inner continental shelf, Florida to Long Island," in *Shelf Sediment Transport: Process and Pattern*, edited by D. J. P. Swift, D. B. Duane, and O. H. Pilkey (Dowden, Hutchinson & Ross, Stroudsburg, PA, 1972), pp. 447–498.
[17]E. L. Hamilton, "Sound velocity and related properties of marine sediments, North Pacific," J. Geophys. Res. **75**, 4423–4446 (1970).
[18]M. D. Richardson, K. B. Briggs, R. I. Ray, and W. H. Jahn, "Environmental support for high-frequency acoustic experiments conducted at the Quinault Range off the Washington coast, 28 April–1 May 1983," NORDA Rep. No. 132, Naval Ocean Research and Development Activity, NSTL Station, MS (1986).
[19]K. B. Briggs, P. Fleischer, R. I. Ray, W. B. Sawyer, D. K. Young, M. D. Richardson, and S. Stanic, "Environmental support for a high-frequency acoustic bottom backscatter experiment off Charleston, South Carolina, 17–28 June 1983," NORDA Rep. No. 130, Naval Ocean Research and Development Activity, NSTL Station, MS (1986).
[20]R. L. Folk and W. C. Ward, "Brazos River bar, a study in the significance of grain size parameters," J. Sediment. Petrol. **27**, 3–26 (1957).
[21]We use the term "gravel" not as the commonly used descriptive term for small rocks, but as the conventional term in the Wentworth particle size classifications (shells and shell fragments greater than 2 mm in diameter).
[22]D. B. Percival, Applied Physics Laboratory, University of Washington, private communication (1985).
[23]P. Bloomfield, *Fourier Analysis of Time Series: An Introduction* (Wiley, New York, 1976).
[24]D. Middleton, "Underwater acoustic scattering," Scientific and engineering studies, Naval Underwater Systems Center, **1** (1987).
[25]A. Papoulis, *Probability, Random Variables, and Stochastic Processes* (McGraw-Hill, New York, 1984).
[26]R. J. Urick, "A statistical model for the fluctuation of sound transmission in the sea," Tech. Rep. No. 75-18, Naval Surface Weapons Center, White Oak, Silver Springs, MD (1975).
[27]D. R. Jackson, D. P. Winebrenner, and A. Ishimaru, "Application of the composite roughness model to high-frequency bottom backscattering," J. Acoust. Soc. Am. **79**, 1410–1422 (1986).
[28]D. R. Jackson, "Third report on TTCP bottom scattering measurements: model development," APL-UW Rep. No. 8708, APL-University of Washington, Seattle, WA (1987).
[29]M. D. Richardson, "Spatial variability of surficial shallow water geoacoustic properties," in *Ocean Seismo-Acoustics*, edited by T. Akal and J. M. Berkson (Plenum, New York, 1986), pp. 527–536.